Lab on a Chip

PAPER

Cite this: *Lab Chip*, 2020, **20**, 3051

Development of elastic artificial vessels with a digital pulse flow system to investigate the risk of restenosis and vasospasm†‡

Yalei Lv, §[a] Guoqiang Li, §[a] Hongyu Peng,§[b] Yanping Liu,[a] Jingru Yao,[a] Gao Wang,[a] Jianfeng Sun,[a] Jinghua Liu,[b] Hongfei Zhang,[c] Guo Chen *[a] and Liyu Liu *[a]

The postoperative risk of stenosis is a complex issue, with risk factors including the status of human umbilical vein endothelial cells, the shear stress of dynamic blood flow, and blood physiology. Current research would benefit from *in vitro* models that can mimic the microenvironment of living vessels, to study the response of endothelial cells to stent placement. In this study, we constructed a digital pulse flow system based on a group of programmable solenoid valves, to mimic dynamic blood flows in the left coronary artery. Elastic artificial vessels, with internally cultured endothelial cells, were used to simulate vessel function and physiology. Based on this novel platform, we systematically explored cell proliferation and function in artificial vessels implanted with bare metal stents or drug-eluting stents, using unstented vessels as controls, under static and pulse flow conditions. The results indicate that the natural shear stresses of dynamic blood flow actually benefit endothelial cell attachment and proliferation. And drug-eluting stents showed stronger inhibition of cell proliferation than bare metal stents, but had a more negative effect on the synthesis of nitric oxide synthase (NOS), suggesting that drug elution might reduce the postoperative risk of restenosis, while increasing the risk of vasospasm. The results suggest that stent evaluation should include both the risk of restenosis and the effect on endothelial cells. Our simulation establishes a realistic *in vitro* model for pathological studies of restenosis and vasospasm, shows potential for evaluation of new stent designs, and could help develop individualised therapies for patients with atherosclerosis.

Received 22nd May 2020,
Accepted 17th July 2020

DOI: 10.1039/d0lc00533a

rsc.li/loc

Introduction

Cardiovascular disease affects the heart and blood vessels, causing huge morbidity and 1/3 of mortality worldwide.[1–4] The causes of the diseases, such as atherosclerosis, thrombus and stenosis, are quite different. For example, stenosis is one of the most common cardiovascular diseases. As vessel walls are subjected to shear stress from pulsed flow, which directly affects the endothelial cells, lipid plaque accumulates under the vessel endothelial layer, causing atherosclerosis, narrowing the arteries, and eventually hindering blood flow.[5] The phenomena of vasoconstriction and vasodilatation induce periodic forces of traction and contraction on endothelial cells, which lead to various pathological reactions and cause further harm *via* atherosclerosis.[6,7] The heart delivers blood to its own cardiac muscle *via* the coronary circulation,[8–10] as shown in Fig. 1A, starting from the aortic root and distributing into the left and right branches on the heart surface. Coronary arteries are composed of the aorta, left coronary artery, right coronary artery, circumflex artery, and left anterior descending artery.[11] Because most coronary arteries are deeply imbedded in myocardial tissues, their contractility is important for coronary blood flow, particularly to tissues of the left ventricle, where stenosis most frequently occurs.[12–16] In the clinic, percutaneous coronary intervention (PCI) is one of the most common treatment methods for stenosis. Balloon-expandable stents can be placed locally, where inflation can reduce stenosis and improve blood flow.[17] At the early stage of PCI, a vessel expanded solely by balloon inflation would be prone to recurrence of stenosis, or 'restenosis'. This phenomenon is mainly related to the elastic recoil of the vessel, as well as neointimal hyperplasia.[18] To avoid vessel recoil, a bare metal

[a] *Chongqing Key Laboratory of Soft Condensed Matter Physics and Smart Materials, College of Physics, Chongqing University, Chongqing 401331, China. E-mail: wezer@cqu.edu.cn, lyliu@cqu.edu.cn*
[b] *Department of Cardiology, Beijing Anzhen Hospital, Capital Medical University, Beijing 100029, China*
[c] *Hygeia International Cancer Hospital, Chongqing 401331, China*

† Y. L., L. L., H. P., G. C., G. L., J. L. and H. Z. designed the research; Y. L. and G. L. performed the research; Y. L., G. L., Y. L., J. Y., G. W., J. S., J. L., H. P., G. C. and L. L. analysed the data; Y. L., G. L., L. L., H. P. and G. C. wrote the paper.

‡ Electronic supplementary information (ESI) available. See DOI: 10.1039/d0lc00533a

§ Y. L., G. L., and H. P. contributed equally to this work.

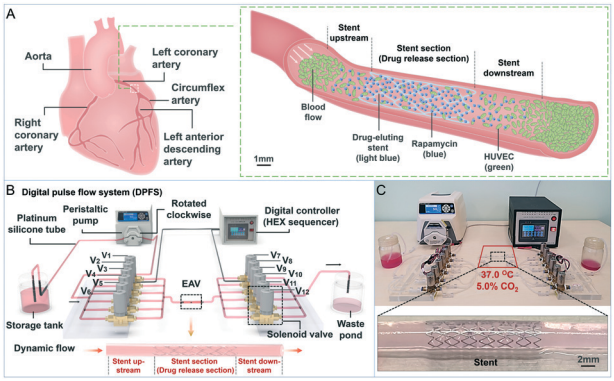

Fig. 1 (A) Left: An illustration of the human heart and coronary arteries. The coronary arteries consist of the aorta, left coronary artery, right coronary artery, circumflex artery, and left anterior descending artery. Right: A schematic diagram of the internal cross-section of a part of the blood vessel in the white box of the left coronary artery, in which a stent containing drugs (rapamycin) is placed. The intravascular part is divided into three sections: the drug-eluting stent upstream section, the stent (light blue) section, and the stent downstream section. Blood as a medium allows diffusion of drugs (rapamycin, blue) to the upper and lower edges of the stent, and the drug concentration is highest in the stent area. In the area furthest away from the stent, the concentration of the drug decreased, and the inhibiting effect of the proliferation of HUVECs (green) also decreased, and the cell density increased accordingly. The white arrow shows the direction of blood flow. (B) Schematic diagram of the DPFS. The device consists of a peristaltic pump, storage tank, EAV, solenoid valves, digital control system, and platinum silicone tube. The EAV (black box) was implanted with a coronary stent. (C) The real DPFS device and EAV with a stent. In the experiment, the EAV was placed in a 37.0 °C, 5.0% CO_2 environment.

stent (BMS) was developed. However, BMS implantation may greatly damage the vessel wall, resulting in detachment of endothelial cells and laceration of the tunica intima, and may also activate vascular smooth muscle cells (VSMCs). VSMCs migrate to the intima for proliferation, transit into the synthetic phenotype, and eventually cause neointimal hyperplasia and restenosis.[19,20] In addition, the BMS can also lead to local hydrodynamic changes in the implanted region, which are another cause of restenosis.[20,21] An improvement came with the invention of a drug-eluting stent (DES), which is regarded as an outstanding technological advance in the development of PCI. Antiproliferative drugs, such as rapamycin and its derivatives and paclitaxel, diffuse from the stent and are able to inhibit local VSMC proliferation and significantly reduce the occurrence of restenosis.[22] However, as the DES has moved into wider clinical use, an increasing amount of evidence has revealed some side effects. Antiproliferative drugs appear to inhibit endothelial cell proliferation and migration, delay vascular endothelialisation, and may cause late-stage stent thrombosis.[22–25] In addition, vasospasm and very late stent failure, after DES implantation, are also related to some form of damage to endothelial cells, brought about by the DES.[26–29] It is apparent that stent implantation, especially the DES, has complex effects on blood vessels. In theory, this is the composite effect of pulsed blood flow, the metallic stent, and the antiproliferative drugs. However, almost all *in vitro* studies focus on addressing a single aspect of disease, which is a long way from taking a 'real world' approach. The fundamental constraint on the research is that an ideal *in vitro* comprehensive experimental system is currently lacking, a system that can mimic the vessel microenvironment (dynamic flows, stents, and drugs) and facilitate evaluation of each PCI factor. Based on these principles, this study seeks to design a digital pulse flow system (DPFS) to mimic the dynamic pulse flow in the left coronary artery. We constructed elastic artificial vessels (EAVs), based on transparent and biocompatible polydimethylsiloxane (PDMS), and human umbilical vein endothelial cells (HUVECs) were cultured inside, to mimic vessel physiology. After EAVs were implanted with each type of stent, and in combination with fluorescence microscopy, our system was able to quantitatively explore the performance of HUVECs against factors of shear flow, periodic vessel deformation, and different stent types, by monitoring their spatial-dependent proliferation and cellular function. This comprehensive system has not only led to an *in vitro* approach for research into restenosis, but also establishes a controllable platform for observation and quantitative analysis, to investigate the postoperative risks of restenosis and vasospasm from stent implantation of different types.

Experimental methods

DPFS design and construction

To accurately simulate the dynamic flow of the left coronary artery *in vitro*, we designed and developed a DPFS, shown in Fig. 1B and C. The device consists of a peristaltic pump (MASTERFLEX® L/S, USA), a storage tank, an EAV (2.5 mm inner diameter, 21 mm length), 12 independent solenoid valves (VDW21-6G-1-M5, Japan), a home-made digital controller, a platinum silicone tube (Tygon 3350, ABW00002, USA; 1.6 mm inner diameter, 0.8 mm thickness), and other accessory components. The peristaltic pump provides continuous power and control of the fluid flow inside the DPFS channels. The 12 solenoid valves are divided into two groups: the upstream solenoid valves (V1–V6) and the downstream valves (V7–V12). According to the experimental requirements, four solenoids (V5, V6, V11, and V12) function as backup solenoid valves. The digital controller controls the status of the opening and closing of the solenoid valves, connected to the channel through the programming sequence in the HEX sequencer.

The details of the digital programming principles of the HEX sequencer are shown in the ESI.‡ During the experiment, the output flow rate of the peristaltic pump was set to 50.0 μL min^{-1}. The pump head was rotated clockwise, so the RPMI-1640 medium was drawn continuously from the storage tank and then passed through the upstream solenoid valves, the EAV, and the downstream solenoid valves, in sequence, before finally flowing into the waste pond. During the experiments, the platinum silicone tube and EAV section between the upstream and downstream solenoid valves were placed inside a constant-temperature cell incubator (37.0 °C, 5.0% CO_2) to

ensure an optimal *in vivo* cultivation environment for HUVECs. The EAV was taken out for microscopic imaging only when HUVEC observations were performed.

EAV preparation and modification

PDMS with good biocompatibility was selected to prepare EAVs as models for culturing HUVECs. The details of EAV preparation and characterisation can be found in the ESI.‡ Due to its hydrophobicity, the raw PDMS surface is not conducive to cell attachment and growth, and the inner wall of the EAV requires hydrophilic treatment to enhance cell adhesion. First, the residual white oil (food grade, Shanghai Xiangping Industrial Co., Ltd., China) attached to the inner wall of the EAV was washed off with a 10.0% w/w sodium dodecyl sulphate solution (AR, Shanghai McLean Biochemical Technology Co., Ltd., China). Then, the EAV was rinsed with 75.0% ethanol and dried. After that, it was irradiated with ultraviolet light (intensity $>$ 180 μW cm^{-3}) for 3 h, to allow its inner wall to sterilize and adhere.[30,31] Following that, a fibronectin solution (Fibronectin, F2006, Sigma-Aldrich, USA) at a concentration of 100 μg mL^{-1} was injected into the EAV with a pipette. It was then placed in a cell incubator (37.0 °C, 5.0% CO_2) for 12 h. The finished EAV, with strong inner wall adhesion, was obtained after extracting the residual solution of fibronectin.

Cell culture and seeding inside EAVs

The HUVECs, labelled with green fluorescent protein (GFP), were obtained from ATCC (Virginia, USA). In order to obtain GFP expression, the CD513B plasmid that carried the green fluorescent protein was co-transfected with modified HIV lentivirus plasmids (VSVG, pLP1 and pLP2) into 293 T cells for packaging the infective virus. Then, the HUVECs were infected with the virus and maintained in complete medium containing 2.0 μg ml^{-1} puromycin for 4–8 weeks after infection. The cells were maintained in RPMI-1640 (Corning, NY, USA) supplemented with 10.0% (v/v) foetal bovine serum (E600001, BBI, China) and 1.0% (v/v) penicillin/streptomycin (30-002-CI, Corning, USA).[32] All cells were cultured in an incubator at 37.0 °C with 5.0% CO_2. To construct biocompatible models, our modified EAVs were seeded with HUVECs. A cell suspension, with a density of 1.0 × 10^5 cells per mL, was injected into the modified EAV and placed in the cell incubator for 8 min. After the cells were deposited at the bottom of the EAV, the cell suspension was extracted and the EAV was turned clockwise by 90°. After that, the first step was repeated four times, until HUVECs were evenly seeded on the inner wall of the EAV. The final density of the cells was approximately 4.0 × 10^8 cells per m^2. The reason for afterwards HUVEC seeding in EAVs was to avoid possible damage to the integrity of the cell layer along stent implantation.

Analysis and conversion of the left coronary artery blood flow curve

In order to use our DPFS to simulate dynamic blood flow in the human heart, it was necessary to acquire the parameters of

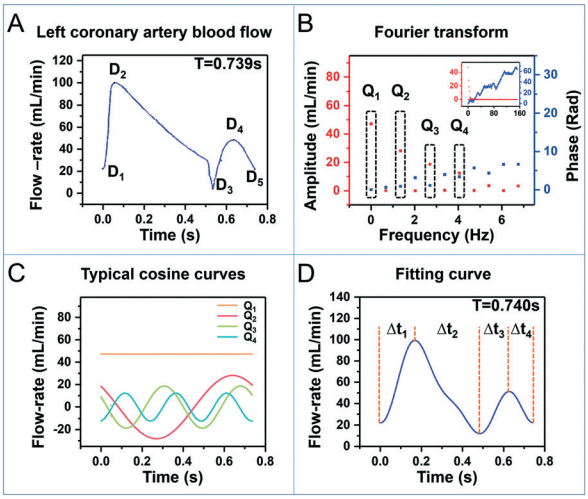

Fig. 2 Analysis of the human left coronary artery blood flow curve. (A) The blood flow curve of a single cycle (0.739 s) is divided into four stages: D1–D2 (0.058 s), D2–D3 (0.477 s), D3–D4 (0.102 s), and D4–D5 (0.102 s). (B) The amplitude and phase of the first eleven low-frequency cosine functions obtained by Fourier transform. The inset shows the amplitude and phase of all 227 cosine functions. (C) The first four cosine curves Q_1, Q_2, Q_3, and Q_4 with the largest amplitudes. (D) The four cosine curves are combined into a simplified waveform curve, and the curve is divided into four time stages, according to the trend of the curve with time, corresponding to the four time stages of the curve in Fig. 2(A).

blood flow, characteristic of human blood vessels. The blood flow curve of the human left coronary artery was used as a reference, as shown in Fig. 2A.[33] Its characteristic parameters were extracted *via* a Fourier transform, serving as the basis for subsequent programming. Fig. 2B presents the Fourier transform analysis of the curve shown in Fig. 2A, using Origin 2017 (Origin Lab, USA). The horizontal, left vertical, and right vertical axes, respectively, indicate the frequency (Hz), amplitude (mL min^{-1}), and phase (rad). The main graph illustrates the characteristic parameters of the first eleven low-frequency components. To simplify the question, the first four sets of cosine curves with the largest amplitudes are selected and combined to represent the original flow curve, and the corresponding waveforms (Q_1, Q_2, Q_3, and Q_4) are shown in Fig. 2C. Their expressions are listed below:

$$Q_1 = 47.166 \quad (1)$$

$$Q_2 = 28.154\cos(8.487t + 0.872) \quad (2)$$

$$Q_3 = 18.704\cos(16.974t + 1.098) \quad (3)$$

$$Q_4 = 12.408\cos(25.461t + 3.365) \quad (4)$$

Fig. 2C shows that the Q_1 (orange) curve serves as a stable baseline and determines the main flow rate. The frequencies and phases of Q_2 (red), Q_3 (green), and Q_4 (blue) jointly control the period and nonlinear characteristics of the flow curve. Fig. 2D shows the fitting curve, with a period of 0.740

s, after the combination of the four waveforms. The curve is divided into four stages. The flow rate increases at stage Δt_1 = 0.160 s, corresponding to the D1–D2 region in Fig. 2A. During stage Δt_2 = 0.340 s, corresponding to D2–D3 in Fig. 2A, the flow rate decreases. At stage Δt_3 = 0.140 s, the flow rate increases again, corresponding to D3–D4 in Fig. 2A. At stage Δt_4 = 0.100 s, corresponding to D4–D5 in Fig. 2A, the flow rate decreases. The flow trends and corresponding time intervals of these four stages provided a design basis for the subsequent experiments using our DPFS, for programming the digital controller to control the execution status and timing of the solenoid valves.

Comparative analysis of the fluid curve acquired from the DPFS and the human left coronary artery blood flow curve

To confirm that the DPFS constructed in this study can simulate the blood flow of the human left coronary artery *in vitro*, we used the HUVEC culture medium as the experimental fluid and tested its pulse flow curve with the system. A comparison with the blood flow curve of the human left coronary artery demonstrates the feasibility of our DPFS to simulate real blood flow. Combining the typical response behaviour of the single solenoid valve (see the ESI‡) with the characteristics of the simplified curve in Fig. 2D (the trends and durations of the four stages), we developed a programming strategy for the DPFS (Fig. 3A) to simulate the blood flow of the human left coronary artery, through repeated debugging. More details of the controlling principle

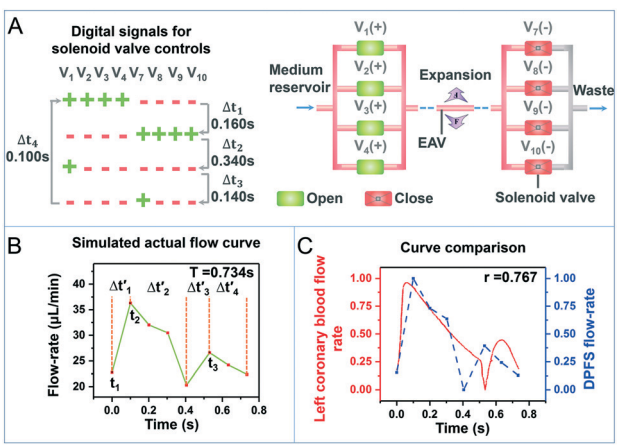

Fig. 3 (A) Left: The command strategy of the solenoid valve controller based on the trend and time interval of the four time periods of the curve in Fig. 2(D). Right: A schematic diagram of the principle of the DPFS. EAV = simulated vessel. '+' indicates that the valve is open and fluid can pass. '–' means that the valve is closed and the fluid is blocked. When the valves on the left are all opened, and the valves on the right are all closed, the fluid pressure inside the EAV increases, and the EAV expands outward. (B) The actual flow rate curve in the EAV, obtained in the experiment following the strategy above. t_1, t_2, and t_3 indicate the starting point, first peak, and second peak, respectively. (C) Comparison of the correlation between the actual flow rate (blue dotted line) and the human left coronary blood flow curve. The correlation coefficient is 0.767, indicating a strong correlation between them.

can be found in the ESI.‡ Fig. 3A shows that valves V1, V2, V3, and V4 are located upstream of the EAV, while V7, V8, V9, and V10 are located downstream. According to the strategy, the upstream valves are all fully opened (indicated by the green plus sign), while all the downstream valves are closed (illustrated by the red minus sign) during the first 0.160 s. During this time, the fluid is blocked by the downstream valves, and the fluid pressure in the EAV increases, making the EAV wall expand (the directions of fluid movement and EAV expansion are illustrated in the right inset of Fig. 3A). The upstream valves are then closed, and the downstream valves are opened, for 0.340 s. During this time, the fluid in the EAV flows out from the downstream valves, releasing the pressure and making the EAV contract inwards. The EAV expands and retracts periodically, along with the periodic change of fluid pressure, by continuous repetition of the above operations. To explore the difference between the blood flow curve of the human left coronary artery and the flow curve simulated in the experiment, the flow rate of the EAV was monitored, in real time, with a microfluidic flow meter (MFCS, FLUIGENT, France), and the results are shown in Fig. 3B. The actual flow curve has also been divided into four stages, similar to the stages in Fig. 2A. At stage $\Delta t_{1'}$ = 0.100 s, corresponding to D1–D2 in Fig. 2A, the flow rate increases. At stage $\Delta t_{2'}$ = 0.305 s, the flow rate decreases, corresponding to D2–D3 in Fig. 2A. At stage $\Delta t_{3'}$ = 0.126 s, the flow rate increases again, corresponding to D3–D4 in Fig. 2A. At stage $\Delta t_{4'}$ = 0.203 s, corresponding to D4–D5 in Fig. 2A, the flow rate decreases. The experimental flow curve demonstrates the same trends as the blood flow curve of the left coronary artery. Specifically, both curves exhibit a large peak, followed by a small peak, in each cycle. Correlational analyses were also conducted to quantitatively analyse the correlation between the blood flow curve of the human left coronary artery (Fig. 2A) and the simulated flow curve (Fig. 3B) using IBM SPSS (Statistics 24.0). The analysis steps are as follows. First, the flow rate Q was normalised, with the following formula:

$$Q^* = \frac{Q - Q_{\min}}{Q_{\max} - Q_{\min}}$$

where Q^* is the normalised flow rate. Then, the data were loaded into IBM SPSS (Statistics 24.0). The result of correlation analysis shows that the correlation coefficient r between the two curves is 0.767. This indicates that the actual flow at the EAV is strongly correlated with the blood flow curve of the human left coronary artery. It should also be noted that there is a difference in the time correspondence between these two curves, possibly due to the delay of the solenoid valves and the different response times between real blood flow *in vivo* and the flow of culture medium in an EAV.

Fluorescence imaging and analysis of HUVECs

The growth and proliferation of HUVECs in the EAVs are key parameters to investigate the stent influence. For comparison, all the images need to be captured under the

same conditions and processed in unified methods. Regarding imaging conditions, an inverted microscope (Ti-E, Nikon, Japan) was employed to measure HUVEC proliferation. With a microscopic emission wavelength of 535 nm, an excitation wavelength of 480 nm, an exposure time of 800 ms and a PHL (4 × 0.13) phase difference, the fluorescence of HUVECs was imaged every 24 h for 192 h in total. For the sake of comparison, image normalization is needed. As the colour values of the images were in the range of 0–255 grey values, their LUT values were adjusted to lower the overall brightness, that is, the ranges of LUTs for all the images were set from 0 to 5×10^4. Hence, the same standards were adopted from imaging to post-processing. Finally, the noise to background ratio, which depends on the threshold, should be normalized for the images as well. In detail, images at a specific EAV area were taken every 24 h and nine images in total were obtained, namely 0 h to 192 h. In consideration of the background noise inside, the graythresh function was used in MATLAB to obtain the grey threshold value of 0.21 from the specific 192 h image. And this value was used as a standard threshold for all the images, *i.e.*, the grey values less than the 0.21 threshold were set to 0 in order to exclude the influence of background noise.

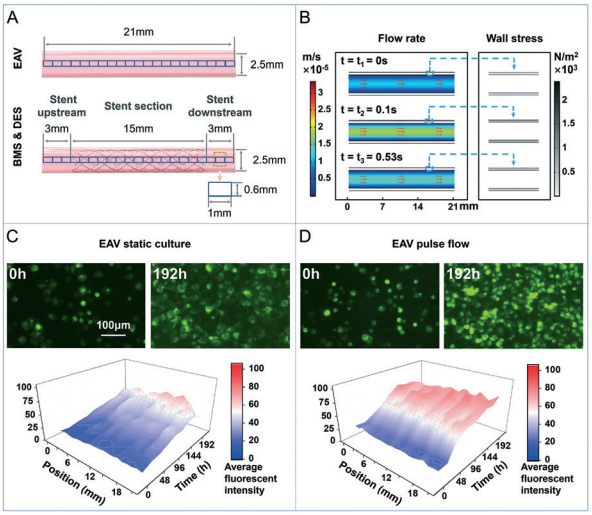

Fig. 4 (A) The inner surface of the artificial vessel was divided into 21 areas to quantitatively process the images of HUVEC proliferation. (B) Numerical distribution of the fluid velocity and wall stress in EAV at three typical points t_1, t_2, and t_3 of the actual pulsed fluid flow curve (Fig. 3(B)). (C) and (D) The growth status of HUVECs in the EAV from 0–192 h under static and pulse flow conditions, respectively. The average fluorescence intensity of cells in the whole artificial blood vessel varies with time (0–192 h) and space (0–21 mm). It can be concluded that HUVECs proliferate significantly faster under dynamic flow conditions than in static culture.

Results and discussion

Promotion of HUVEC attachment and proliferation under pulse flow conditions

We prepared identical EAVs (length 21 mm, O. D 3.5 mm, I.D 2.5 mm) and implanted them with BMS and DES stents of clinical grade (length: 15 mm, Partner, China). Then, the HUVECs were introduced inside and cultured on their inner walls to simulate the *in vivo* vessel environment after stent implantation. Previous research has demonstrated that stent implantation is likely to cause not only vessel restenosis, but also an 'edge effect' in the zones upstream and downstream of the stent.[34,35] For detailed analysis, shown in Fig. 4A from left to right, the EAV with stent implantation is divided into three sections: upstream (length: 3 mm), the stent itself (length: 15 mm) and downstream (length: 3 mm). For convenience of observation and quantification of HUVEC growth, each section was divided into several units, each of which was 1.0 mm in length and 0.6 mm in width (blue).

The DPFS generates a dynamic pulse flow that periodically applies pressure to the inner wall, resulting in its corresponding deformation. The observation of the deformation can be found in the ESI‡ and Movie SI1. According to the dynamic flow curve in the EAV (Fig. 3B), COMSOL Multiphysics (Multiphysics 5.3a, Comsol, Sweden) was used to simulate dynamic flow and the distribution of wall shear strain (WSS). A detailed, finite element analysis from COMSOL can be found in the ESI.‡ Three typical time points (t_1, t_1, and t_3) are selected, with their corresponding pulse flow distributions, and the WSS of the EAV is shown in Fig. 4B. In detail, at $t_1 = 0$ s, the average flow rate is relatively small and is approximately 1.0×10^{-5} m s^{-1} in the centre of the vessel. The WSS at this time is approximately 0.5×10^3 N m^{-2}. At $t_2 = 0.1$ s, the average flow rate increases and the flow rate in the centre reaches approximately 2.0×10^{-5} m s^{-1}, while the WSS increases to approximately 1.0×10^3 N m^{-2}. When $t_3 = 0.53$ s, the average flow rate reduces to approximately 1.5×10^{-5} m s^{-1}, and the corresponding WSS reduces to approximately 0.5×10^3 N m^{-2}. The full COMSOL dynamic simulation results are shown in Movie SI2.‡ In general, the average flow rate in the EAV and its corresponding WSS first increased and then reduced, periodically, in a way that matched the experimental results of the real-time EAV flow rate changes in Fig. 3B. Besides, the WSS range is also consistent with clinical *in vivo* values, within the range from 0–6×10^3 N m^{-2}.[36] This result further indicates that the use of EAVs, whose deformation is correlated with the dynamic flow in the channel, presents a satisfactory approach to mimicking vessel bionic properties.

Another key bionic property of EAVs is their ability to allow the culture of HUVECs on the interior surface, which allows the observation and analysis of the development and proliferation of HUVECs in static culture and dynamic flow. Under each of these conditions, interior images of HUVEC development and time–space changes of fluorescence intensity from 0 h to 192 h were captured using the Ti-E inverted microscope (Fig. 4C and D). Previous studies have indicated that the cell number is proportional to the cell fluorescence intensity, therefore the former is represented by the latter *in situ* in EAVs.[37,38] Each experiment was repeated at least three times, and representative data are presented here: At the beginning (0

h), cells in both states exhibited spherical shapes and were uniformly distributed over the inner wall. Over time, the cells attached to the substrate continued to grow and proliferate. Interestingly, by 192 h, the cells under the pulse flow conditions possessed much higher density compared to those in the static state. In order to further quantify the cell spatial development, the cell average fluorescence intensity (CAFI) was calculated and plotted, as an indirect representation of cell growth and proliferation, in each specific zone. The details of HUVEC fluorescence data acquisition and analysis can be found in the ESI.‡ The data show that, in the static state, HUVECs slowly proliferated with time and the CAFI reached 56.9 at 192 h. Meanwhile, cells in the pulse flow exhibited a much faster proliferation rate and its CAFI reached 70.5 at 192 h. This indicates that, although dynamic pulse flow and its resulting shear stress would reduce HUVEC attachment, our experiment proved that pulse flow within a certain range would have the opposite effect, and that periodic and dynamic deformation of the EAV is of benefit to cell attachment and proliferation.[39–41]

Influence of the DES and BMS on HUVEC growth and proliferation

Based on the results discussed above, although the BMS and DES play important roles in the treatment of vascular stenosis by PCI, the clinical data show that they also cause some postoperative risk. For example, the BMS may cause neointimal hyperplasia or restenosis, while the DES may cause vasospasm, late-stage stent thrombosis, and very late stent failure.[22,24,28] In addition, our previous research also showed that hydrodynamics could greatly influence the biological effect of stents.[42] Hence, it could be concluded that a comprehensive experimental platform is needed to integrate drugs and pulse flow conditions, to explore the potential effects of the BMS and DES on HUVECs in the vessel. In order to achieve this goal, we implanted two real stents into EAVs: BMS (316 L stainless steel, metal strut thickness 36 μm, extended diameter 3.0 mm) and DES with rapamycin (316 L stainless steel, metal strut thickness 36 μm, thickness of drug coating 6.0 ± 1.8 μm, drug loading 1.2 μg mm^{-2}, extended diameter 3.0 mm), and analysed their effects on HUVEC growth and proliferation under both static state and pulse flow conditions. The *in vitro* stent implantation process can be found in the ESI.‡ As shown in Fig. 5, in the static state, HUVECs in the EAV-BMS kept proliferating throughout, and the CAFI ≈ 48.8 at 192 h. Interestingly, the edge effect was apparent, in that the CAFI in the stent region (44.8) was smaller than those in the upstream (55.3) and downstream (62.2) sections, as highlighted by the red arrows. This indicates that, although the BMS has been widely applied in the clinic, its metallic impurity and surface charge could inhibit HUVEC proliferation to some degree.[43] However, under pulse flow conditions, after 192 h, the average CAFI in the stent, upstream and downstream regions reached 82.1, which was significantly higher than in the static state. To some extent, this result indicates that the

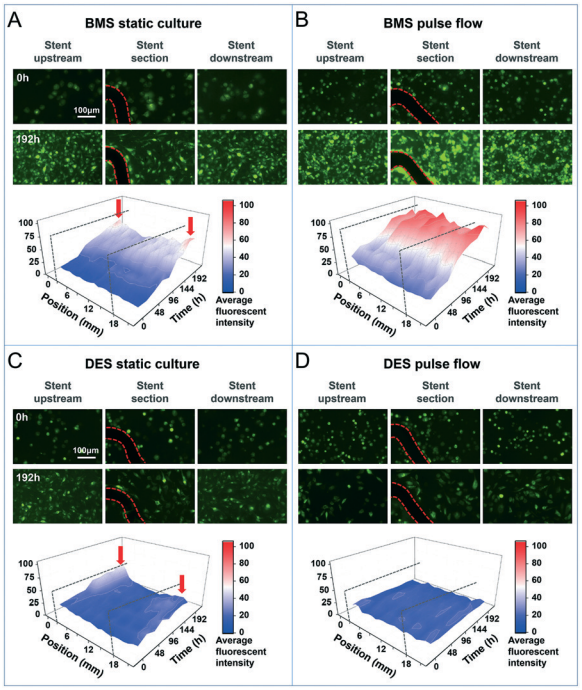

Fig. 5 (A) and (B) are the fluorescence maps of HUVECs in different areas of the wall of the EAV-BMS from 0–192 h under static and pulse flow conditions, respectively. The average fluorescence intensity distribution of HUVECs changes over time (0–192 h) and space (0–21 mm). The black shadow surrounded by the red dotted line indicates the area of the stent structure and, in the calculation of the average fluorescence intensity of cells, data for this region are excluded. (C) and (D) are the fluorescence maps of HUVECs in different regions of the wall of the EAV-DES between 0 h and 192 h under static and pulse flow conditions, and the average fluorescence intensity of HUVECs varies over time (0–192 h) and space (0–21 mm).

hydrodynamic shear stress from pulsed flow has a stronger promotive effect on the HUVECs than the effect of stent inhibition on the cells. Fig. 5C shows that after 192 h in the static state, HUVECs in the EAV-DES stent region showed no obvious proliferation, with CAFI at 16.8. However, the CAFI of HUVECs was higher in the upstream (48.9) and downstream regions (21.5), highlighted by the red arrows. The reason for this may be that, under the static conditions, drug molecules could only spread by diffusion, leading to fairly low drug concentrations upstream and downstream of the stent, resulting in minor inhibition of local HUVECs. In contrast, in dynamic pulse flow (Fig. 5D), HUVEC proliferation was apparently inhibited throughout the entire region. This indicates that forward and backward pulse flow accelerated the rapamycin release from the stent, which rapidly spread upstream and downstream and significantly inhibited HUVECs in the local regions.

Nitric oxide synthase (NOS) analysis of stent HUVECs under pulse flow conditions

The HUVECs, particularly those experienced pulse flow conditions in EAVs, had been proved to be in good condition

with normal physiology *via* immunofluorescence analysis. DAPI, VE-cad and von Willebrand factor (vWF) were stained and imaged using a two-photon confocal microscope (SP8, Leica, Germany). The details can be found in the ESI.‡ In order to directly compare the growth and proliferation of HUVECs between the EAV-BMS stent section and the EAV-DES stent section, under pulse flow conditions, the CAFI of HUVECs at 192 h is plotted in Fig. 6A. The CAFI in the EAV-BMS stent region ≈ 81.2 and that in the EAV-DES stent region ≈ 16.8, while the value for the stent-free EAV ≈ 70.7. This indicates that under conditions of simulated, dynamic blood flow, the DES significantly inhibited HUVEC proliferation, while the BMS had no significant effect on the cells. Not limited to inhibition of HUVEC proliferation, the DES may also affect physiological function. Reports have shown that nitric oxide (NO), an endothelial-derived relaxing factor (EDFR), is broadly involved in the physiology and pathology regulation of the cardiovascular system.[44,45] As shown in Fig. 6B, when acetyl choline (Ach) in the vessel is combined with its receptor, it opens an ion channel to facilitate calcium ion entry into endothelial cells and raises the ion level in the protoplasm. Subsequently, calcium ions combined with calmodulin, and integrated with NOS, form active endothelial nitric oxide synthase (eNOS). This catalyses the oxidation of L-arginine (L-Arg) to L-citrulline (L-Cit) and releases NO. NO then enters nearby VSMCs, *via* diffusion, and is combined with ferrous ions from haem, a cofactor of guanylate cyclase (GC), to form active GC. It then catalyses the change of guanosine triphosphate (GTP) to cyclic guanosine monophosphate (cGMP) and relaxes VSMCs. Therefore, physiologically, HUVECs are able to synthesise NO *via* NOS, to inhibit VSMC shrinkage and maintain normal diastolic and systolic function in the vessel.[44]

However, in pathology, because of the reduction in the number of HUVECs or insufficient function, synthesis of NO is reduced, which leads to possible vessel shrinkage and vasospasm. In short, the NO level in HUVECs is representative of their function, to some degree, and is one of the important parameters to evaluate the effect of the stent type on the postoperative risk of cardiovascular stenosis.[46] However, because of the extreme instability of NO, it is difficult to perform *in situ* measurements in tissues. Currently, most studies attempt to evaluate NO levels indirectly, by the measurement of the NOS concentration in HUVECs. Previous results showed that HUVEC-related eNOS protein would be upregulated under dynamic flow conditions.[47] In our study, in order to analyse the influence of the stent type on NOS, we extracted HUVECs at 192 h, from the EAV, EAV-BMS stent section, and EAV-DES stent section under pulse flow conditions, and measured their NOS concentrations. The method for NOS measurement can be found in the ESI.‡ As Fig. 6C reveals, the average NOS concentration of HUVECs in the EAV, EAV-BMS stent section, and EAV-DES stent section is 10.6, 8.5, and 7.6 μmol L^{-1}, respectively. The data show that the BMS and DES affect NOS concentrations, to some extent, compared to stent-free EAVs. Specifically, the DES value is smaller than the BMS value. For statistical analysis, IBM SPSS software was used to perform paired sample *t*-test and analyse significant differences in NOS concentration in HUVECs under pulse flow conditions in group–group combinations, *i.e.*, EAV and EAV-BMS, EAV and EAV-DES, and EAV-BMS and EAV-DES, respectively. $P < 0.05$ is considered statistically significant. The EAV-DES with rapamycin exhibits significant influence on the NOS concentration of HUVECs, compared to the EAV-BMS and EAV cases. The result indicates that the DES has more influence on NOS function and may carry higher risk of vasospasm, which is consistent with clinical observations as well.[48]

In summary, implanted stents influence HUVEC proliferation and function in EAVs, indicating that the evaluation of stent prognosis should include not only the influence on the risk of restenosis, but also the effects on HUVEC proliferation and function. Our results show that our system and method can be used to simulate the influence of implanted stents on HUVEC proliferation and NOS function *in vivo*. The influence of the stent on HUVEC proliferation can be directly obtained through the measurement of changes in CAFI. In addition, the examination of the NOS concentration can be used to estimate the decline in HUVEC function caused by stent implantation and to indirectly estimate NO levels in the vessel, in order to investigate the risk of vasospasm. It should be noted that there are a considerable number of clinical studies indicating that vasospasm is more likely in the region downstream of the stent.[29] In the future, we will attempt to measure NOS concentrations accurately in extended regions on either side of the stent, to further evaluate how different types of stents cause HUVEC dysfunction, particularly in the downstream section.

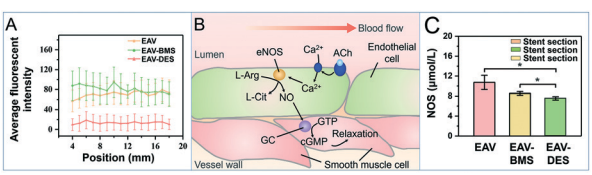

Fig. 6 (A) The fluorescence intensity distributions of HUVECs in the EAV, the stent sections of the EAV-BMS and EAV-DES (15 mm long) at 192 h under pulse flow conditions. (B) Schematic diagram of the mechanism of nitric oxide in endothelial cells to relax blood vessels through smooth muscle cells. (C) Comparison of the concentration of NOS in HUVECs in the EAV and stent sections of the EAV-BMS and EAV-DES under pulse flow conditions. *P-Value is in the range of 0.01–0.05, and $P < 0.05$ indicates statistical significance.

Conclusions

Our study designed and constructed a DPFS for use with EAV models. The DPFS simulates dynamic blood flow *in vitro*, and EAVs were prepared and implanted with two different types of stents: BMS or DES. This comprehensive system provides an *in vitro* research platform that approaches the *in vivo* microenvironment and facilitates a quantitative study on the composite effect of dynamic flow shear stress, the stent type, and related antiproliferative drugs on HUVECs. Our study found that the hydrodynamic shear force and stent type are key factors

influencing HUVECs. Specifically, the normal shear stress of pulsed circulation facilitates HUVEC attachment and proliferation, and its promotion of cell proliferation is much greater than that of static culture. The DES inhibited HUVEC proliferation significantly and delayed the progression of complete endothelialisation. But based on NOS analysis, it was found that the DES could also inhibit the NOS synthesis in HUVECs and cause endothelial cell dysfunction. The adverse effects of rapamycin on cell proliferation and function would increase the risk of vasospasm, stent thrombosis, and very late stent failure. Therefore, the process of selection of appropriate stents for patients with stenosis not only needs to consider the risk of restenosis after stent implantation, but also needs to evaluate the influence of stents on proliferation and function of HUVECs. In addition, for future design and development of novel stents, it is highly recommended to balance their possible postoperative risks comprehensively. New stent designs should be expected to reduce the risk of restenosis while simultaneously maintaining the normal physiology of the HUVECs.

Our studies will continue to use the current DPFS, which has further potential in studies of cardiovascular disease and in clinical applications. In combination with CT angiography image reconstruction and 3-D printing technology, it should be possible to generate a more realistic and complex bifurcated elastic vessel model. The aim will be to achieve better modelling of nonlinear, coronary blood flow, in order to explore the potential for individualised treatment of atherosclerotic lesions. Furthermore, modified culture media incorporating platelets and other blood factors could be introduced into EAVs, for a more realistic approach to analysis of the composite effect of interactions between blood flows, stents, and drugs on HUVECs. In summary, the DPFS together with EAV models provides useful experimental data for exploring cardiovascular restenosis and vasospasm, as well as quantitatively evaluating different types of stents. In the future, this research should facilitate the design of individualised treatment for patients with atherosclerosis.

Conflicts of interest

There are no conflicts to declare.

Acknowledgements

We gratefully acknowledge support from the National Natural Science Foundation of China (11974066, 11674043), the Fundamental and Advanced Research Program of Chongqing (cstc2019jcyj-msxmX0477) and the Fundamental Research Funds for the Central Universities (2019CDYGYB007). Besides, we would like to thank Miss Qin Deng at Analytical and Testing Center of Chongqing University for her assistance with immunofluorescence imaging and analysis.

Notes and references

1 M. Mcclellan, N. Brown, R. M. Califf and J. J. Warner, *Circulation*, 2019, **139**, e44–e54.
2 M. Kanbay, L. A. Ertuglu, B. Afsar, E. Ozdogan, Z. S. Kucuksumer, A. Ortiz, A. Covic, M. Kuwabara, D. Z. I. Cherney, D. H. van Raalte and D. de Zeeuw, *Diabetes, Obes. Metab.*, 2019, **21**, 2368–2383.
3 P. L. Schnall, M. Dobson and P. Landsbergis, *Int. J. Health Serv.*, 2016, **46**, 656–692.
4 M. Mollenhauer, D. Mehrkens and V. Rudolph, *Nitric Oxide*, 2018, **78**, 146–153.
5 C. H. Tan, N. Muhamad and M. M. A. B. Abdullah, *IOP Conf. Ser.: Mater. Sci. Eng.*, 2017, **209**, UNSP012031.
6 J. J. Chiu, S. Usami and S. Chien, *Ann. Intern. Med.*, 2009, **41**, 19–28.
7 V. Thondapu, C. V. Bourantas, N. Foin, I. K. Jang, P. W. Serruys and P. Barlis, *Eur. Heart J.*, 2017, **38**, 81–92.
8 C. Seiler, *Heart*, 2003, **89**, 1352–1357.
9 F. Kajiya, M. Zamir and S. Carlier, *Ann. Biomed. Eng.*, 2005, **33**, 1728–1734.
10 M. Stoller and C. Seiler, *Swiss Med. Wkly.*, 2015, **145**, w14154.
11 A. Sevrukov, V. Jelnin and G. T. Kondos, *AJR, Am. J. Roentgenol.*, 2001, **177**, 1437–1445.
12 S. J. Park and Y. H. Kim, *World J. Cardiol.*, 2010, **2**, 78–88.
13 V. Sucato, A. Sansone, G. Coppola, C. Nugara, L. Ajello, P. Candela, P. Di Girolamo, S. Asciutto, M. Farinella, D. Piraino, A. Rotolo, G. Andolina, S. Novo and P. Assennato, *Int. J. Cardiol.*, 2014, **172**, e273–e275.
14 C. N. Ionescu and T. J. Donohue, *Conn. Med.*, 2009, **73**, 333–335.
15 G. Barone-Rochette, G. Vanzetto, A. Fluttaz, S. Marliere, H. Bouvaist, M. Durand, O. Chavanon, D. Blin and J. Machecourt, *Int. J. Cardiol.*, 2011, **148**, 394–396.
16 G. Sleilaty, P. de Lentdecker, F. Thaler, A. Ceddaha, V. Jebara, E. Lansac and M. Debauchez, *Ann. Thorac. Surg.*, 2010, **90**, 628–629.
17 D. Mylotte, R. A. Byrne, R. Iijima and A. Kastrati, *Minerva Cardioangiol.*, 2008, **56**, 493–510.
18 M. Herten, G. B. Torsello, E. Schonefeld and S. Stahlhoff, *Vasc. Health Risk Manage.*, 2016, **12**, 341–356.
19 H. Ando, A. Suzuki, S. Sakurai, S. Kumagai, A. Kurita, K. Waseda, H. Takashima and T. Amano, *Heart Vessels*, 2017, **32**, 531–538.
20 K. C. Koskinas, Y. S. Chatzizisis, A. P. Antoniadis and G. D. Giannoglou, *J. Am. Coll. Cardiol.*, 2012, **59**, 1337–1349.
21 S. T. Hsiao, T. Spencer, L. Boldock, S. D. Prosseda, I. Xanthis, F. J. Tovar-Lopez, H. Van Beusekamp, R. Y. Khamis, N. Foin and N. Bowden, *Cardiovasc. Res.*, 2016, **112**, 689.
22 Y. He, J. Wang, W. Yan and N. Huang, *RSC Adv.*, 2013, **4**, 212–221.
23 S. Bangalore, S. Kumar, M. Fusaro, N. Amoroso, M. J. Attubato, F. Feit, D. L. Bhatt and J. Slater, *Circulation*, 2012, **125**, 2873–2891.
24 N. Guo, F. Chen, J. Zhou, Y. Fang, H. Li, Y. Luo and Y. Zhang, *J. Cardiovasc. Pharmacol.*, 2015, **66**, 338–346.
25 F. Alfonso, R. A. Byrne, F. Rivero and A. Kastrati, *J. Am. Coll. Cardiol.*, 2014, **63**, 2659–2673.

26 N. Matsumoto, K. Nagao, A. Hirayama and S. Kasama, *BMJ Case Rep.*, 2014, **2014**, bcr2013202996.
27 H. Shibutani, Y. Akita, Y. Matsui, M. Yoshinaga and M. Karakawa, *BMC Cardiovasc. Disord.*, 2016, **16**, 236.
28 M. J. Hung, K. H. Hsu, N. C. Chang, S. Tsimikas and M. Y. Hung, *Int. J. Cardiol.*, 2015, **179**, 252–255.
29 C. M. Gibson, D. J. Cohen, E. A. Cohen, H. K. Lui, S. A. Murphy, S. J. Marble, M. Kitt, T. Lorenz and J. E. Tcheng, *Am. J. Cardiol.*, 2001, **87**, 1293–1295.
30 Y. Berdichevsky, J. Khandurina, A. Guttman and Y. H. Lo, *Sens. Actuators, B*, 2004, **97**, 402–408.
31 H. F. Lv, W. P. Yan, Z. H. Liu and J. C. Li, *Spectrosc. Spectral Anal.*, 2016, **36**, 1033–1037.
32 C. Bian, J. Lin, X. C. Li, Y. F. Wang, H. Q. Hu and P. Chen, *Scand. J. Clin. Lab. Invest.*, 2007, **67**, 619–631.
33 D. N. Zhu, T. H. Wang, Z. Q. Luo, Y. F. Guan and X. L. Jin, *Physiology*, Beijing: People's Medical Publishing House, 2013, pp. 145–146.
34 K. Wakabayashi, R. Waksman and N. J. Weissman, *Circ.: Cardiovasc. Interventions*, 2012, **5**, 305–311.
35 K. Waseda, J. Ahko, H. Kaneda, A. Miyazawa and Y. Shimada, *Circ. J.*, 2008, **72**, 534–537.
36 C. Xu, X. Liu, G. Wu, Y. He, L. Shu and C. Lin, *Chin. J. Biomed. Eng.*, 2016, **35**, 428–434.
37 A. Krtolica, C. Ortiz de Solorzano, S. Lockett and J. Campisi, *Cytometry*, 2002, **49**, 73–82.
38 T. A. McCaffrey, L. A. Agarwal and B. B. Weksler, *In Vitro Cell. Dev. Biol.*, 1988, **24**, 247–252.
39 T. Ahsan and R. M. Nerem, *Tissue Eng., Part A*, 2010, **16**, 3547–3553.
40 J. Ando, H. Nomura and A. Kamiya, *Microvasc. Res.*, 1987, **33**, 62–70.
41 Z. Xiao, B. Zhang, E. Zhang, W. Xu, Y. Shi and Y. Guo, *J. Biomed. Eng.*, 2011, **28**, 157–162.
42 H. Wang, J. Liu, X. Zheng, X. Rong, X. Zheng, H. Peng, Z. Silber-Li, M. Li and L. Liu, *Sci. Rep.*, 2015, **5**, 10945.
43 S. Jin, X. Qi, B. Zhang, Z. Sun, B. Zhang, H. Yang, T. Wang, B. Zheng, X. Wang, Q. Shi, M. Chen, L. Ren, K. Yang and H. Zhong, *Sci. Rep.*, 2017, **7**, 17394.
44 S. Ma and C. C. Ma, *Vasc. Pharmacol.*, 2014, **63**, 63–70.
45 R. O. Cannon, *Clin. Chem.*, 1998, **44**, 1809–1819.
46 T. Suzuki, K. Okumura, T. Sone, T. Kosokabe and T. Hayakawa, *Int. J. Cardiol.*, 2002, **86**, 71–76.
47 J. Tao, Z. Yang, J. M. Wang, C. Tu and S. R. Pan, *Cardiology*, 2006, **106**, 82–88.
48 G. Nakazawa, M. Nakano, F. Otsuka, J. N. Wilcox, R. Melder, S. Pruitt, F. D. Kolodgie and R. Virmani, *Circ.: Cardiovasc. Interventions*, 2011, **4**, 38–46.